
VideoMambaPro: A Leap Forward for Mamba in Video Understanding

Hui Lu*, Albert Ali Salah, Ronald Poppe
Utrecht University

Abstract

Video understanding requires the extraction of rich spatio-temporal representations, which transformer models achieve through self-attention. Unfortunately, self-attention poses a computational burden. In NLP, Mamba has surfaced as an efficient alternative for transformers. However, Mamba’s successes do not trivially extend to computer vision tasks, including those in video analysis. In this paper, we theoretically analyze the differences between self-attention and Mamba. We identify two limitations in Mamba’s token processing: historical decay and element contradiction. We propose VideoMambaPro (VMP) that solves the identified limitations by adding masked backward computation and elemental residual connections to a VideoMamba backbone. VideoMambaPro shows state-of-the-art video action recognition performance compared to transformer models, and surpasses VideoMamba by clear margins: 7.9% and 8.1% top-1 on Kinetics-400 and Something-Something V2, respectively. Our VideoMambaPro-M model achieves 91.9% top-1 on Kinetics-400, only 0.2% below InternVideo2-6B but with only 1.2% of its parameters. The combination of high performance and efficiency makes VideoMambaPro an interesting alternative for transformer models. Code is available at <https://github.com/hotfinda/VideoMambaPro>.

1 Introduction

Video understanding is a challenging task, requiring models that can extract rich spatio-temporal representations from video inputs. Transformers are powerful neural networks capable of effectively capturing temporal and spatial information from videos [20, 29, 50]. Therefore, most current state-of-the-art models for video understanding are based on transformers [41, 54]. At the core of transformers is self-attention [49], which learns the self-alignment between tokens in an input sequence by estimating the relative importance of a given token with respect to all other tokens. This long-range token dependency accounts for much of the success of transformer models [5, 49].

However, the cost involved in computing the self-attention is high, which eventually limits the application of powerful transformer models in practical settings [17]. Recently, alternative models with lower-cost operators have been proposed in the language processing domain, including S4 [13], RWKV [36], and RetNet [45]. Among these methods, Mamba [11] shows the best performance on long-range and causal tasks such as language understanding [31] and content-based reasoning [35].

Motivated by the favorable computational cost, researchers have recently extended Mamba from the NLP domain to the computer vision domain. The core adaptation involved splitting the input image into multiple regions and embedding these as continuous tokens [62]. For video understanding, the recently proposed VideoMamba [19] extracts key frames from videos as the continuous input sequence. However, compared to previous transformer-based methods, VideoMamba’s performance

*Corresponding author

on video benchmarks is significantly lower. For example, VideoMamba achieves 82.4% top-1 on Kinetics-400, compared to 85.2% for VideoMAE [47], indicating room for improvement.

In this paper, we first analyze differences in the feature extraction capabilities of transformers and Mamba. We identify two limitations of Mamba when applied to video understanding: historical decay and element contradiction. We then extend VideoMamba to mitigate these limitations. The proposed VideoMambaPro addresses historical decay through masked backward computation in the bi-directional Mamba process, allowing the network to better handle historical tokens. To tackle element contradiction, we introduce residual connections to Mamba’s matrix elements. VideoMambaPro consistently improves the performance of VideoMamba on video understanding tasks, positioning it as a strong, efficient competitor to transformers. In summary, our contributions are:

- We derive a formal representation of Mamba from the perspective of self-attention and identify two limitations of Mamba in the video analysis domain.
- We propose VideoMambaPro, which effectively addresses the identified limitations present in Mamba for the video understanding task.
- We report strong performance on video action recognition benchmarks compared to state-of-the-art transformer methods, and surpass the original VideoMamba by clear margins.

We first discuss related work. Then, we provide our theoretical analysis, before introducing the VideoMambaPro architecture. Experiments are summarized in Section 5 and we conclude in Section 6

2 Related Work

Transformers. One core aspect of transformers is self-attention [49]. It achieves long-range interactions by measuring the similarity between tokens. Self-attention was introduced in the computer vision domain for tasks such as image recognition [26, 44] and object detection [6, 59]. Subsequent works (e.g., [8, 21, 47, 55]) extended vision transformers to the video domain, to achieve superior performance. However, the mechanism of self-attention, which relies on similarity measurement, introduces significant computational overhead. The bulk of the computational cost arises from matrix multiplications for all input tokens with each other.

Alternative models. Recent work has introduced alternative models with reduced computational complexity, while maintaining the advantages of self-attention [30, 40, 60]. SOFT [30] propose to utilize Gaussian kernel function to replace the dot-product similarity, which enables a full self-attention matrix to be approximated via a low-rank matrix decomposition. Combiner [40] proposes to utilize the structured factorization to approximate full self-attention, realizing low computation and memory complexity.

RWKV [36] combines parallel self-attention training with efficient recurrent neural network (RNN) inference using a linear attention mechanism. It proposes a model architecture called Receptance Weighted Key Value (RWKV) to achieve parallel computation and constant-level computational and memory complexity. RetNet [45] contains another variant of self-attention, by dividing the input into multiple chunks. Within each chunk, the self-attention mechanism can be computed in parallel, while information is transmitted between chunks based on an RNN.

The S4 model completely abandons self-attention and, instead, builds upon a state space model [13]. Instead of performing individual matrix multiplications for tokens to obtain a similarity matrix, it enables the network to directly learn a global HiPPO (high-order polynomial projection operator) matrix to handle relations between tokens. Additionally, for the simultaneous input of multiple tokens, S4 proposes a convolutional processing approach, enabling parallel training and thereby accelerating the training process. Based on S4, Mamba [11] proposes a selection mechanism where, for each input token, a unique HiPPO matrix [12] is generated. This allows the model to selectively process input tokens, enabling it to focus on or ignore specific inputs. Due to Mamba’s strong representation ability in NLP, and linear-time complexity, it has garnered widespread attention as a promising alternative to transformers. In the computer vision domain, researchers have proposed Vision Mamba [62] and VMamba [27] for tasks such as image classification and object detection.

In the video domain, VideoMamba [19] has been proposed. However, its performance is lower than expected, with limited understanding of the causes. We argue that a systematic, mathematical analysis of Mamba from the perspective of self-attention could reveal shortcomings of Mamba’s

inner workings. Better understanding of these limitations allow us to develop improvements, and to close the accuracy performance gap with transformers, while enjoying the efficiency of Mamba.

3 Theoretical Analysis

First, we revisit Mamba from the perspective of self-attention. Then, we analyze its limitations for video understanding. We propose VideoMambaPro to address these limitations in Section 4.

3.1 Mamba from the perspective of self-attention

Self-attention. Given an input sequence $\mathbf{X} := [\mathbf{x}_1, \dots, \mathbf{x}_N] \in \mathbb{R}^{N \times D_x}$ of N feature vectors of depth D_x , self-attention [49, 61] computes the output sequence \mathbf{Y} from \mathbf{X} following two steps:

Step 1: Compute similarity matrix. The input sequence \mathbf{X} is linearly projected onto three different subspaces: query $\mathbf{Q} \in \mathbb{R}^{N \times D}$, key $\mathbf{K} \in \mathbb{R}^{N \times D}$, and value $\mathbf{V} \in \mathbb{R}^{N \times D_v}$:

$$\mathbf{Q} = \mathbf{X} \mathbf{W}_Q^\top; \mathbf{K} = \mathbf{X} \mathbf{W}_K^\top; \mathbf{V} = \mathbf{X} \mathbf{W}_V^\top; \quad (1)$$

with $\mathbf{W}_Q, \mathbf{W}_K \in \mathbb{R}^{D \times D_x}$, and $\mathbf{W}_V \in \mathbb{R}^{D_v \times D_x}$ the corresponding weight matrices. Specifically, $\mathbf{Q} := [\mathbf{q}_1, \dots, \mathbf{q}_N]^\top$, $\mathbf{K} := [\mathbf{k}_1, \dots, \mathbf{k}_N]^\top$, and $\mathbf{V} := [\mathbf{v}_1, \dots, \mathbf{v}_N]^\top$ with vectors $\mathbf{q}_i, \mathbf{k}_i, \mathbf{v}_i$ for $i = 1, \dots, N$ the query, key, and value vectors, respectively, for input vector i . Based on \mathbf{Q} and \mathbf{K} , similarity matrix $\mathbf{S} \in \mathbb{R}^{N \times N}$ contains the correlations between all query and key vectors:

$$\mathbf{S} = \text{softmax}(\mathbf{Q} \mathbf{K}^\top / \sqrt{D}) \quad (2)$$

The softmax function is applied to each row of the matrix $(\mathbf{Q} \mathbf{K}^\top / \sqrt{D})$. The similarity matrix \mathbf{S} can be denoted as:

$$\mathbf{S} = \begin{bmatrix} s_{11} & s_{12} & s_{13} & \cdots & s_{1N} \\ s_{21} & s_{22} & s_{23} & \cdots & s_{2N} \\ s_{31} & s_{32} & s_{33} & \cdots & s_{3N} \\ \cdots & \cdots & \cdots & \ddots & \vdots \\ s_{N1} & s_{N2} & s_{N3} & \cdots & s_{NN} \end{bmatrix} \quad (3)$$

where each component s_{ij} ($i, j = 1, \dots, N$) represents the similarity score between \mathbf{q}_i and \mathbf{k}_j .

Step 2: Compute output based on similarity matrix. Output sequence $\mathbf{Y} := [\mathbf{y}_1, \dots, \mathbf{y}_N]^\top$ is then calculated as:

$$\mathbf{Y} = \mathbf{S} \mathbf{V} \quad (4)$$

Following this equation, each output vector \mathbf{y}_i ($i = 1, \dots, N$) can be written in vector form as:

$$\mathbf{y}_i = \sum_{j=1}^N s_{ij} \mathbf{v}_j \quad (5)$$

Any output vector \mathbf{y}_i is a linear combination of vectors \mathbf{v}_j ($j = 1, \dots, N$), with similarity score s_{ij} serving as coefficient. The larger the similarity score, the greater the influence of \mathbf{v}_j on \mathbf{y}_i [42].

Mamba. State Space Models (SSMs) serve as the foundation of Mamba [11], and they are based on continuous systems that map a 1D function or sequence, $x(t) \in \mathbb{R}^L \rightarrow y(t) \in \mathbb{R}^L$ to output sequence $y(t)$ through a hidden state $h(t) \in \mathbb{R}^N$. Formally, SSM implements the mapping as²:

$$h(t) = \mathbf{A}h(t-1) + \mathbf{B}x(t), \quad (6)$$

$$y(t) = \mathbf{C}h(t) \quad (7)$$

where $\mathbf{A} \in \mathbb{R}^{N \times N}$ is the evolution matrix of the system, and $\mathbf{B} \in \mathbb{R}^{N \times 1}$, $\mathbf{C} \in \mathbb{R}^{N \times 1}$ are the projection matrices. Often, inputs are discrete rather than a continuous function $x(t)$. Therefore,

²The original SSM [13] employs $h'(t) = \mathbf{A}h(t) + \mathbf{B}x(t)$, with $h(t)$ the hidden state inherited from the previous time step $t-1$, and $h'(t)$ represents the updated current hidden state, replacing $h(t)$. Considering this approach may lead to ambiguity, we have adopted the updated description as in Mamba to avoid ambiguity.

Mamba performs discretization, effectively creating a discrete version of the continuous system. A timescale parameter Δ is used to transform the continuous parameters \mathbf{A}, \mathbf{B} into their discrete counterparts $\bar{\mathbf{A}}, \bar{\mathbf{B}}$, and the transformation typically employs the zero-order hold method [58]. This process is expressed as:

$$\bar{\mathbf{A}} = \exp(\Delta \mathbf{A}), \quad (8)$$

$$\bar{\mathbf{B}} = (\Delta \mathbf{A})^{-1}(\exp(\Delta \mathbf{A}) - \mathbf{I}) \cdot \Delta \mathbf{B} \quad (9)$$

$$h_t = \bar{\mathbf{A}}h_{t-1} + \bar{\mathbf{B}}x_t, \quad (10)$$

$$y_t = \mathbf{C}h_t. \quad (11)$$

Considering that parameters $\bar{\mathbf{A}}, \bar{\mathbf{B}}, \mathbf{C}$ in the original SSM are independent of the input data $x(t)$ and cannot be tailored to specific input data, Mamba employs a Selective Scan Mechanism as its core operator. More precisely, three functions $S_B(x), S_C(x), S_\Delta(x)$ are introduced to associate parameters $\bar{\mathbf{B}}, \mathbf{C}, \Delta$ in Equations 8–11 to the input data x . Based on $S_\Delta(x)$, $\bar{\mathbf{A}}$ can also be associated with the input data x . For example, given the input x_1 , functions $S_\Delta(x)$ will produce the corresponding $\bar{\mathbf{A}}_1$ based on Equation 8, and functions $S_B(x)$ and $S_\Delta(x)$ will produce the corresponding $\bar{\mathbf{B}}_1$ based on Equation 9. $\bar{\mathbf{C}}_1$ is obtained based on function $S_C(x)$. Following Equations 10 and 11, we analyze the process to obtain output sequence \mathbf{Y} when given an input sequence $\mathbf{X} := [x_1, \dots, x_N] \in \mathbb{R}^{N \times D_x}$ of N feature vectors. The hidden state of each vector is denoted as:

$$h_1 = \bar{\mathbf{B}}_1 x_1 \quad (12)$$

$$h_2 = \bar{\mathbf{A}}_2 h_1 + \bar{\mathbf{B}}_2 x_2 = \bar{\mathbf{A}}_2 \bar{\mathbf{B}}_1 x_1 + \bar{\mathbf{B}}_2 x_2 \quad (13)$$

$$h_3 = \bar{\mathbf{A}}_3 h_2 + \bar{\mathbf{B}}_3 x_3 = \bar{\mathbf{A}}_3 \bar{\mathbf{A}}_2 \bar{\mathbf{B}}_1 x_1 + \bar{\mathbf{A}}_3 \bar{\mathbf{B}}_2 x_2 + \bar{\mathbf{B}}_3 x_3 \quad (14)$$

...

$$h_N = \bar{\mathbf{A}}_N h_{N-1} + \bar{\mathbf{B}}_N x_N = \bar{\mathbf{A}}_N \bar{\mathbf{A}}_{N-1} \cdots \bar{\mathbf{A}}_2 \bar{\mathbf{B}}_1 x_1 + \bar{\mathbf{A}}_N \bar{\mathbf{A}}_{N-1} \cdots \bar{\mathbf{A}}_3 \bar{\mathbf{B}}_2 x_2 + \bar{\mathbf{A}}_N \bar{\mathbf{A}}_{N-1} \cdots \bar{\mathbf{A}}_4 \bar{\mathbf{B}}_3 x_3 + \cdots + \bar{\mathbf{A}}_N \bar{\mathbf{B}}_{N-1} x_{N-1} + \bar{\mathbf{B}}_N x_N \quad (15)$$

Equations 12 – 15 can be written in the following matrix form:

$$\mathbf{H} = [h_1, h_2, h_3, \dots, h_N]^\top = \begin{bmatrix} 0 & \bar{\mathbf{B}}_1 & 0 & \cdots & 0 \\ \bar{\mathbf{A}}_2 \bar{\mathbf{B}}_1 & \bar{\mathbf{B}}_2 & 0 & \cdots & 0 \\ \bar{\mathbf{A}}_3 \bar{\mathbf{A}}_2 \bar{\mathbf{B}}_1 & \bar{\mathbf{A}}_3 \bar{\mathbf{B}}_2 & \bar{\mathbf{B}}_3 & \cdots & 0 \\ \vdots & \vdots & \vdots & \ddots & \vdots \\ \bar{\mathbf{A}}_N \bar{\mathbf{A}}_{N-1} \cdots \bar{\mathbf{A}}_2 \bar{\mathbf{B}}_1 & \bar{\mathbf{A}}_N \bar{\mathbf{A}}_{N-1} \cdots \bar{\mathbf{A}}_3 \bar{\mathbf{B}}_2 & \bar{\mathbf{A}}_N \bar{\mathbf{A}}_{N-1} \cdots \bar{\mathbf{A}}_4 \bar{\mathbf{B}}_3 & \cdots & \bar{\mathbf{B}}_N \end{bmatrix} \begin{bmatrix} x_1 \\ x_2 \\ x_3 \\ \vdots \\ x_N \end{bmatrix} \quad (16)$$

For output sequence $\mathbf{Y} := [y_1, \dots, y_N]^\top$, each vector y_i ($i = 1, \dots, N$) can be expressed as:

$$y_N = \bar{\mathbf{C}}_N h_N \quad (17)$$

And in matrix form as:

$$\mathbf{Y} = \begin{bmatrix} \bar{\mathbf{C}}_1 & 0 & 0 & \cdots & 0 \\ 0 & \bar{\mathbf{C}}_2 & 0 & \cdots & 0 \\ 0 & 0 & \bar{\mathbf{C}}_3 & \cdots & 0 \\ \vdots & \vdots & \vdots & \ddots & \vdots \\ 0 & 0 & 0 & \cdots & \bar{\mathbf{C}}_N \end{bmatrix} \begin{bmatrix} h_1 \\ h_2 \\ h_3 \\ \vdots \\ h_N \end{bmatrix} \quad (18)$$

By substituting Equation 16 into Equation 18, we obtain the following expression:

$$\mathbf{Y} = \begin{bmatrix} \bar{\mathbf{C}}_1 & 0 & 0 & \cdots & 0 \\ 0 & \bar{\mathbf{C}}_2 & 0 & \cdots & 0 \\ 0 & 0 & \bar{\mathbf{C}}_3 & \cdots & 0 \\ \vdots & \vdots & \vdots & \ddots & \vdots \\ 0 & 0 & 0 & \cdots & \bar{\mathbf{C}}_N \end{bmatrix} \begin{bmatrix} \bar{\mathbf{B}}_1 & 0 & 0 & \cdots & 0 \\ \bar{\mathbf{A}}_2 \bar{\mathbf{B}}_1 & \bar{\mathbf{B}}_2 & 0 & \cdots & 0 \\ \bar{\mathbf{A}}_3 \bar{\mathbf{A}}_2 \bar{\mathbf{B}}_1 & \bar{\mathbf{A}}_3 \bar{\mathbf{B}}_2 & \bar{\mathbf{B}}_3 & \cdots & 0 \\ \vdots & \vdots & \vdots & \ddots & \vdots \\ \bar{\mathbf{A}}_N \bar{\mathbf{A}}_{N-1} \cdots \bar{\mathbf{A}}_2 \bar{\mathbf{B}}_1 & \bar{\mathbf{A}}_N \bar{\mathbf{A}}_{N-1} \cdots \bar{\mathbf{A}}_3 \bar{\mathbf{B}}_2 & \bar{\mathbf{A}}_N \bar{\mathbf{A}}_{N-1} \cdots \bar{\mathbf{A}}_4 \bar{\mathbf{B}}_3 & \cdots & \bar{\mathbf{B}}_N \end{bmatrix} \begin{bmatrix} x_1 \\ x_2 \\ x_3 \\ \vdots \\ x_N \end{bmatrix} \quad (19)$$

Which can be expressed as:

$$\mathbf{Y} = \mathbf{C}(\mathbf{M}\mathbf{X}) \quad (20)$$

where \mathbf{C} and \mathbf{M} represent the first and second term on the right-hand side of Equation 19, respectively. Recall Equation 4 that the result \mathbf{Y} obtained by self-attention processing can be expressed as:

$$\mathbf{Y} = \mathbf{S}\mathbf{V} = (\mathbf{S}\mathbf{X})\mathbf{W}_V^\top \quad (21)$$

From the perspective of self-attention, by comparing Equations 20 and 21, the essence of Mamba is to generate a matrix \mathbf{M} similar to similarity matrix \mathbf{S} , such that the result of $\mathbf{M}\mathbf{X}$ is also based on the correlation between vectors of \mathbf{X} . Although the final result of $\mathbf{M}\mathbf{X}$ is left multiplied by a mapping matrix \mathbf{C} , while the result of $\mathbf{S}\mathbf{X}$ is right multiplied by a mapping matrix \mathbf{W}_V^\top , the geometric meanings of the two are the same.

3.2 Limitations of Mamba in video understanding

From the perspective of self-attention, the concept of Mamba is similar: both center around similarity matrices. We now analyze the differences between the similarity matrices of Mamba and self-attention, and discuss the limitations of Mamba in the context of the video understanding task.

Limitation 1: Historical decay. Matrix \mathbf{M} in Equation 20 corresponds to the second right-hand term in Equation 19, which is a lower triangular matrix of the form:

$$\mathbf{M} = \begin{bmatrix} m_{11} & 0 & 0 & \cdots & 0 \\ m_{21} & m_{22} & 0 & \cdots & 0 \\ m_{31} & m_{32} & m_{33} & \cdots & 0 \\ \vdots & \vdots & \vdots & \ddots & \vdots \\ m_{N1} & m_{N2} & m_{N3} & \cdots & m_{NN} \end{bmatrix} \quad (22)$$

By comparing \mathbf{M} with matrix \mathbf{S} in self-attention, we find that outputs in Mamba favor more recent information, because the more weights are zero the earlier the token is observed. For example, for input $[\mathbf{x}_1, \mathbf{x}_2, \mathbf{x}_3]$, the output $\mathbf{M}\mathbf{x}_1$ in Mamba is $m_{11}\mathbf{x}_1$ while the output $\mathbf{S}\mathbf{x}_1$ is $s_{11}\mathbf{x}_1 + s_{12}\mathbf{x}_2 + s_{13}\mathbf{x}_3$ in self-attention. This indicates that, in Mamba, the influence of earlier observed tokens on the final result is greatly diminished. We refer to this limitation as historical decay.

In the NLP domain, more recent dialogue information often has more impact on the final judgment, so this effect is acceptable. However, in the computer vision domain, the order of the tokens has less meaning. Previous works such as Vision Mamba [62] and VMamba [27] have partly mitigated this issue by processing the token sequence in both forward and backward directions. This produces better results but no work has explained why this is effective.

When processing bi-directionally, the results generated from input forward tokens $[\mathbf{x}_1, \dots, \mathbf{x}_N]$, denoted as $\mathbf{M}_f\mathbf{X}$, and the results generated from input backward tokens $[\mathbf{x}_N, \dots, \mathbf{x}_1]$, denoted as $\mathbf{M}_b\mathbf{X}$, are linearly combined to generate the final result $\mathbf{M}_{bi}\mathbf{X}$ with \mathbf{M}_{bi} being a dense matrix. As a result, the influence of historical information on the result is increased, consequently leading to better results.

For example, for the input tokens $[\mathbf{x}_1, \mathbf{x}_2, \mathbf{x}_3]$, $\mathbf{M}_f\mathbf{X}$ and $\mathbf{M}_b\mathbf{X}$ can be expressed as:

$$\mathbf{M}_f\mathbf{X} = \begin{bmatrix} f_{11} & 0 & 0 \\ f_{21} & f_{22} & 0 \\ f_{31} & f_{32} & f_{33} \end{bmatrix} \begin{bmatrix} \mathbf{x}_1 \\ \mathbf{x}_2 \\ \mathbf{x}_3 \end{bmatrix} = \begin{bmatrix} h_{1f} \\ h_{2f} \\ h_{3f} \end{bmatrix}, \quad \mathbf{M}_b\mathbf{X} = \begin{bmatrix} b_{33} & 0 & 0 \\ b_{23} & b_{22} & 0 \\ b_{13} & b_{12} & b_{11} \end{bmatrix} \begin{bmatrix} \mathbf{x}_3 \\ \mathbf{x}_2 \\ \mathbf{x}_1 \end{bmatrix} = \begin{bmatrix} h_{3b} \\ h_{2b} \\ h_{1b} \end{bmatrix} \quad (23)$$

where f_{ij} represents the similarity score during the forward process, and b_{ij} is the similarity score in the backward direction. After bi-directional computation, with the outputs linearly combined, the results are expressed as:

$$\begin{aligned} h_1 &= h_{1f} + h_{1b} = f_{11}\mathbf{x}_1 + b_{13}\mathbf{x}_3 + b_{12}\mathbf{x}_2 + b_{11}\mathbf{x}_1 \\ h_2 &= h_{2f} + h_{2b} = f_{21}\mathbf{x}_1 + f_{22}\mathbf{x}_2 + b_{23}\mathbf{x}_3 + b_{22}\mathbf{x}_2 \\ h_3 &= h_{3f} + h_{3b} = f_{31}\mathbf{x}_1 + f_{32}\mathbf{x}_2 + f_{33}\mathbf{x}_3 + b_{33}\mathbf{x}_3 \end{aligned} \quad (24)$$

We can write Equation 24 in matrix form:

$$\begin{bmatrix} h_1 \\ h_2 \\ h_3 \end{bmatrix} = \begin{bmatrix} f_{11} + b_{11} & b_{12} & b_{13} \\ f_{21} & f_{22} + b_{22} & b_{23} \\ f_{31} & f_{32} & f_{33} + b_{33} \end{bmatrix} \begin{bmatrix} \mathbf{x}_1 \\ \mathbf{x}_2 \\ \mathbf{x}_3 \end{bmatrix} = \mathbf{M}_{bi} \begin{bmatrix} \mathbf{x}_1 \\ \mathbf{x}_2 \\ \mathbf{x}_3 \end{bmatrix} \quad (25)$$

The bi-directional computation transforms the original matrix \mathbf{M} from a lower triangular matrix to a dense matrix \mathbf{M}_{bi} , thereby capturing more historical information and effectively avoiding the historical decay. When extending to the case of N input tokens $[\mathbf{x}_1, \dots, \mathbf{x}_N]$, \mathbf{M}_{bi} can be written as

$$\mathbf{M}_{bi} = \begin{bmatrix} f_{11} + b_{11} & b_{12} & b_{13} & \dots & b_{1N} \\ f_{21} & f_{22} + b_{22} & b_{23} & \dots & b_{2N} \\ f_{31} & f_{32} & f_{33} + b_{33} & \dots & b_{3N} \\ \vdots & \vdots & \vdots & \ddots & \vdots \\ f_{N1} & f_{N2} & f_{N3} & \dots & f_{NN} + b_{NN} \end{bmatrix} \quad (26)$$

The diagonal elements of \mathbf{M}_{bi} contain duplicates of the similarity between a token and itself. For example, f_{33} and b_{33} each represent the similarity between token \mathbf{x}_3 and itself. Consequently, the similarity is effectively doubled which weakens the association with other tokens. One possible approach is to adjust \mathbf{M}_f and \mathbf{M}_b using a weight coefficient z through a linear combination. However, learning such a parameter z that weakens the diagonal elements without affecting other elements might be challenging.

Limitation 2: Element contradiction. By analyzing the non-zero elements m_{ij} in \mathbf{M} of Equation 19, it can be summarized that:

$$m_{ij} = \bar{\mathbf{A}}_i m_{i-1j} \quad (27)$$

After multiple iterations, the above equation results in implicit consideration of the correlation between previous tokens and token j when computing the correlation between token i and token j . As a result, m_{ij} exhibits stronger contextual dependencies compared to the elements s_{ij} in the matrix \mathbf{S} . This might explain why Mamba achieves better performance than transformers in the field of NLP. While this is advantageous in the NLP domain, for the computer vision domain, input tokens often lack semantic connections. The consideration of the influence of other tokens on each element, can lead to significant drawbacks.

We often observe an interleaved token structure when processing images. Tokens that “belong together” might not be subsequently processed. For example, in an image classification task, input tokens $[\mathbf{x}_1, \mathbf{x}_2, \mathbf{x}_3]$ might represent image regions $[dog, other, dog]$. Ideally, m_{31} should be a high value, and m_{21} should be low. According to Equation 27, $m_{31} = \bar{\mathbf{A}}_3 m_{21}$, which requires the network to set $\bar{\mathbf{A}}_3$ to a high value to meet the requirement on m_{31} . However, in doing so, $m_{32} = \bar{\mathbf{A}}_3 m_{22}$ would also become larger because m_{22} is also high. But, theoretically, m_{32} should be low. This leads to an element contradiction. Especially for video understanding, such contradictions are common because most video regions contain background and other irrelevant information, making relevant tokens sparse. Consequently, the performance of Mamba applied to video analysis tasks is underwhelming [19, 23, 57].

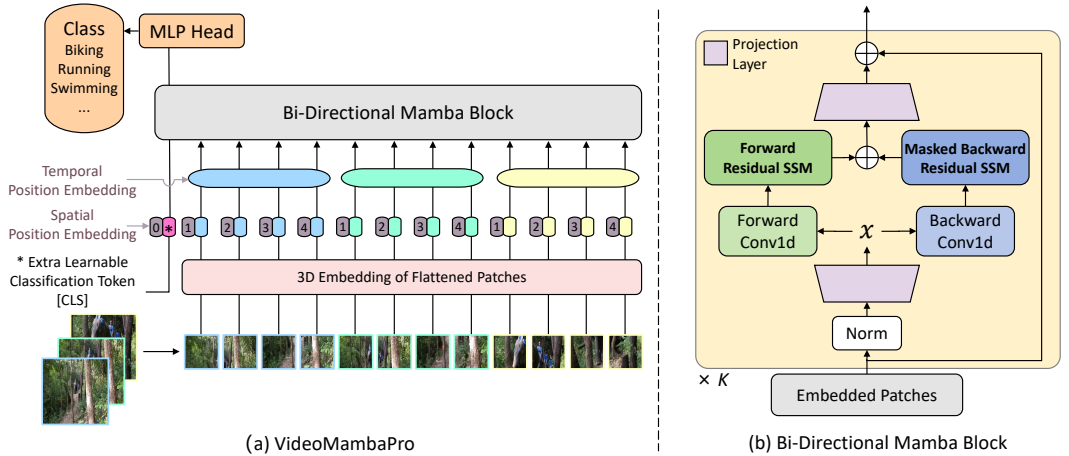


Figure 1: (a) Framework of VideoMambaPro with bi-directional Mamba blocks. (b) In each bi-directional Mamba block, we employ Forward Residual SSM and Masked Backward Residual SSM.

4 VideoMambaPro

We propose two adaptations to VideoMamba [19] to address the two identified limitations: historical decay and element contradiction. The resulting architecture is termed VideoMambaPro (VMP).

To address historical decay, we keep the result of $\mathbf{M}_f \mathbf{X}$ unchanged but we use masked computation during the backward process. Specifically, we assign a mask to the diagonal elements of \mathbf{M}_b , setting their values to 0, and then proceed with the calculations in Equations 22–25. We thus eliminate the duplicate similarity on the diagonal, without affecting other elements. The final \mathbf{M}_{bi} is expressed as:

$$M_{bi} = \begin{bmatrix} f_{11} & b_{12} & b_{13} & \cdots & b_{1N} \\ f_{21} & f_{22} & b_{23} & \cdots & b_{2N} \\ f_{31} & f_{32} & f_{33} & \cdots & b_{3N} \\ \vdots & \vdots & \vdots & \ddots & \vdots \\ f_{N1} & f_{N2} & f_{N3} & \cdots & f_{NN} \end{bmatrix} \quad (28)$$

To solve the element contradiction issue, we propose residual SSM, which is inspired by the idea of residual connections to distribute the requirement for $\bar{\mathbf{A}}_i$ in m_{ij} across multiple $\bar{\mathbf{A}}_i$. This helps to avoid contradictions caused by interleaved sequence structures. For example, for the previous mentioned input sequence $[x_1, x_2, x_3]$, which represents image regions $[dog, other, dog]$, we let $m_{31} = \bar{\mathbf{A}}_3 m_{21} + \bar{\mathbf{A}}_3$. This way, the requirement for a single $\bar{\mathbf{A}}_3$ can be split into two parts, thus avoiding contradictions. This can be expressed as:

$$m_{ij} = \bar{\mathbf{A}}_i m_{ij-1} + \bar{\mathbf{A}}_i \quad (29)$$

Based on these two solutions, we propose our VideoMambaPro framework, based on VideoMamba [19] and illustrated in Figure 1. Given an input video $\mathbf{X}^v \in \mathbb{R}^{3 \times T \times H \times W}$, we first use a 3D convolution with a $1 \times 16 \times 16$ size kernel to convert \mathbf{X}^v into L non-overlapping patch-wise tokens $\mathbf{X}^p \in \mathbb{R}^{L \times C}$, where $L = t \times h \times w$ ($t = T, h = \frac{H}{16}, w = \frac{W}{16}$). Because SSM is sensitive to token positions, and in line with VideoMamba, we include a learnable spatial position embedding $\mathbf{p}_s \in \mathbb{R}^{(hw+1) \times C}$ and a temporal position embedding $\mathbf{p}_t \in \mathbb{R}^{t \times C}$. Input tokens \mathbf{X} are expressed as:

$$\mathbf{X} = [\mathbf{X}_{cls}, \mathbf{X}] + \mathbf{p}_s + \mathbf{p}_t \quad (30)$$

where \mathbf{X}_{cls} is a learnable classification token positioned at the beginning of the sequence. The input tokens \mathbf{X} pass through K Mamba blocks, and the final layer’s [CLS] token is used for video classification, after normalization and linear projection.

	Method	Pre-train data	Input	Crops	Params	FLOPs	Top-1	Top-5
Transformer	MViTv2-L [24]	IN-21K	40×312^2	5×3	218M	42.2T	86.1	97.0
	VideoMAE-H [47]	IN-21K	16×224^2	5×3	633M	17.9T	86.6	97.1
	MAE-H [8]	IN1K+K400+K600-1.9M	16×224^2	4×3	632M	25.1T	86.8	97.2
	MaskFeat-L [55]	IN-21K	64×224^2	4×3	218M	45.5T	87.0	97.4
	EVL-L/14 [25]	CLIP-400M	32×336^2	3×3	67M	19.1T	87.7	—
	X-CLIP-L/14 [32]	CLIP-400M	16×336^2	4×3	453M	37.0T	87.7	—
	MTV-H [56]	IN-21K+WTS-60M	32×224^2	4×3	1120M	44.5T	89.1	98.2
	MTV-H [56]	IN-21K+WTS-60M	32×280^2	4×3	1330M	73.6T	89.9	98.3
	InternVideo-1B [54]	CLIP-400M+Hybrid-12M ¹	64×224^2	16×4	1300M	86.2T	91.1	98.9
	InternVideo2-1B [53]	LAION-300M+Hybrid-414M ²	16×224^2	16×4	$\sim 1000M$	—	91.6	—
	InternVideo2-6B [53]	LAION-300M+Hybrid-414M ²	16×224^2	16×4	5903M	—	92.1	—
	Mamba	VideoMamba-Ti	IN-1K	32×224^2	4×3	7M	0.4T	78.8
VideoMamba-S		IN-1K	32×224^2	4×3	26M	1.6T	81.5	95.2
VideoMamba-M		IN-1K	32×224^2	4×3	74M	4.8T	82.4	95.7
VideoMambaPro-Ti (ours)		IN-1K	32×224^2	4×3	7M	0.4T	85.8	96.9
VideoMambaPro-S (ours)		IN-1K	32×224^2	4×3	24M	1.5T	88.5	98.1
VideoMambaPro-M (ours)		IN-1K	32×224^2	4×3	69M	4.6T	90.3	98.5
VideoMambaPro-M (ours)		IN-1K+CLIP-400M	32×224^2	4×3	69M	4.6T	91.7	98.9
VideoMambaPro-M (ours)		IN-1K+CLIP-400M	32×384^2	4×3	69M	13.3T	91.9	98.9

Table 1: Performance on K400. Best results in **bold**, and second best results underlined. We report crops (temporal \times spatial) and TFLOPs for inference. —: numbers not reported.

¹ WebVid2M/10M+HowTo100M+K710+SSv2+AVA V2.2, and self-collected videos.

² KMash2M+WebVid2M/10M+InternVid40M+LLaVA2.1M, and self-collected videos.

5 Experiments

We introduce experiment setup, followed by our main results and comparisons with the state-of-the-art. In Section 5.3 and 5.4 we compare against VideoMamba model variants and presents statistical tests, respectively. We investigate the effect of each of the two innovations separately in an ablation study in Section 5.5. Finally, we analyze the computation cost in Section 5.6.

5.1 Experimental setup

Datasets. We evaluate VideoMambaPro on five video benchmarks: (a) Kinetics-400 (K400) [3]. K400 comprises $\sim 240\text{K}$ training and $\sim 20\text{K}$ validation videos, each with an average duration of 10 seconds and categorized into 400 classes. (b) Something-Something V2 (SSv2) [10] includes $\sim 160\text{K}$ training and $\sim 20\text{K}$ validation videos. The videos in SSv2 have an average duration of 4 seconds and there are 174 motion-centric classes. (c) UCF-101 [43] is a relatively small dataset, consisting of $\sim 9.5\text{K}$ training and $\sim 3.5\text{K}$ validation videos. (d) HMDB51 [18] is also a compact video dataset, containing $\sim 3.5\text{K}$ training and $\sim 1.5\text{K}$ validation videos. (e) AVA [14] is a dataset for spatio-temporal localization of human actions with $\sim 211\text{k}$ and $\sim 57\text{k}$ validation video segments.

Implementation. In line with VideoMamba, we introduce three models with increasing embedding dimension and number of bi-directional Mamba blocks: Tiny, Small, and Middle (details in the supplementary material). To compare with VideoMamba, we pre-train VideoMambaPro on ImageNet-1K (IN-1K). On K400, we also pre-train with IN-1K and CLIP-400M. We fine-tune on the benchmark’s training set and report on the validation set. During pre-training, we follow DeiT [48] and we apply a center crop to obtain the 224^2 size images. We apply random cropping, random horizontal flipping, label-smoothing regularization, mix-up, and random erasing as data augmentations. We use AdamW [28] with a momentum of 0.9, a batch size of 1024, and a weight decay of 0.05. We employ a cosine learning rate schedule during training, 1×10^{-3} initial learning rate over 300 epochs. The fine-tuning settings follow VideoMAE [47]. We resize frames to 224^2 , and use AdamW with a momentum of 0.9 and a batch size of 512. Details in the supplementary materials.

5.2 Comparison with state-of-the-art

K400. Results appear in Table 1. Compared to VideoMamba, our model has slightly fewer parameters and FLOPs. This is primarily because VideoMamba employs an additional projection layer to generate the weight coefficient z to adjust \mathbf{A}_f and \mathbf{A}_b . See the supplementary materials for an architecture comparison. VideoMambaPro outperforms VideoMamba significantly. When pre-trained only on IN-1K, the best-performing VideoMambaPro-M achieves a top-1 accuracy of 90.3%, 7.9% higher than VideoMamba-M. When additionally pre-training on CLIP-400M, we report a top-1 performance of 91.7, surpassing all transformer models except the recent InternVideo2-6B [53]. The latter scores 0.4% better but is trained on more data. With 1.2% of the parameters, VideoMambaPro is much more efficient. The number of FLOPs for InternVideo2 is not reported but compared to the previous InternVideo [54], inference takes only $\sim 5.3\%$ of the FLOPs, while performing 0.8% better. Finally, when we increase the input size, we narrow the gap to InternVideo2-6B to 0.2%.

	Method	Pre-train data	Input	Crops	Params	TFLOPs	Top-1	Top-5
Transformer	UniFormerV1-B [22]	IN-1K	32×224^2	1×3	50M	0.8	71.2	92.8
	BEVT [51]	IN-1K+K400	32×224^2	—	88M	1.0	71.4	—
	MViTv2-B [24]	IN-21K	32×224^2	1×3	51M	0.7	72.1	93.4
	MaskFeat-L [55]	IN-21K	64×312^2	4×3	218M	8.5	75.0	95.0
	VideoMAE-L [47]	IN-21K	32×224^2	1×3	305M	4.3	75.4	95.2
	TubeViT-L [37]	IN-1K	32×224^2	4×3	311M	9.5	76.1	95.2
	InternVideo [54]	See Table 1	64×224^2	16×4	1300M	86.2	<u>77.2</u>	95.9
	InternVideo2 [53]	See Table 1	64×224^2	16×4	5903M	—	77.5	—
Mamba	VideoMamba-S	IN-1K	16×224^2	2×3	26M	0.4	67.6	90.9
	VideoMamba-M	IN-1K	16×224^2	4×3	74M	2.4	68.3	91.4
	VideoMambaPro-S	IN-1K	16×224^2	2×3	24M	0.4	74.3	94.9
	VideoMambaPro-M	IN-1K	16×224^2	4×3	69M	2.3	76.4	<u>95.4</u>

Table 2: Performance on SSv2. Best results in **bold**, second best results underlined. —: not reported.

SSv2. Results appear in Table 2. VideoMambaPro outperforms VideoMamba by 6.7–8.1%. It also outperforms several popular transformer models. Only InternVideo [54] and InternVideo2-6B [53] perform 0.8 and 1.1% better, respectively, but with more pre-training, 18.8-85.6 times more parameters and at least 40 times more FLOPs. In line with the results for K400, we expect that the performance for VideoMambaPro will increase with more pre-training.

Method	Params	UCF-101	HMDB51
VideoMoCo [33]	15M	78.7	49.2
MemDPC [15]	32M	86.1	54.5
Vi ² CLR [4]	9M	89.1	55.7
VIMPAC [46]	307M	92.7	65.9
CORP [16]	32M	93.5	68.0
XDC [2]	33M	94.2	67.1
CVRL [38]	328M	94.4	70.6
GDT [34]	33M	95.2	72.8
MMVFAC [1]	94M	95.2	75.0
VideoMAE [47]	87M	96.1	73.3
MVD-L [52]	87M	97.5	79.7
VideoMAE V2 [50]	1050M	99.6	88.1
VideoMamba-M	74M	93.7	68.9
VideoMambaPro-M	69M	<u>97.9</u>	<u>80.5</u>

Table 3: Results on UCF-101 and HMDB51.

Method	FLOPs	Param	mAP
SlowFast R101 [9]	138G	53M	23.8
HIT [7]	622G	198M	32.6
MViTv2-L [24]	2828G	213M	34.4
ST-MAE-H [8]	1193G	632M	36.2
VideoMAE-L [47]	597G	305M	37.0
MaskFeat [55]	2828G	218M	37.5
VideoMAE-H [47]	1192G	633M	39.5
InternVideo [54]	8733G	1300M	41.0
MVD-H [52]	1192G	633M	41.1
VideoMAE V2 [50]	4220G	1050M	<u>42.6</u>
LART-MViT [39]	3780G	1640M	<u>42.6</u>
Hiera-H [41]	1158G	672M	43.3
VideoMamba-M [20]	200G	74M	37.4
VideoMambaPro-M	192G	69M	42.2

Table 4: Results on AVA V2.2.

UCF-101/HMDB51/AVA V2.2. From Table 3, it shows that VideoMambaPro-M is competitive, and outperforms VideoMamba by 4.2% and 11.6% on UCF-101 and HMDB51, respectively. When pre-trained only on IN-1K, VideoMambaPro-M achieves 42.2 mAP on AVA V2.2, which is 1.1% lower than Hiera-H [41] but with an order of magnitude fewer parameters and FLOPs (see Table 4).

5.3 Comparison with VideoMamba on K400

In Table 5, we compare VideoMamba and VideoMambaPro across model size, pre-train data and input size. The improvements of VideoMambaPro are systematic, in the range of 6.2–8.2%. Interestingly, the performance increase for the larger, better performing, models is not lower despite the smaller margin for improvement. More quantitative results appear in the supplementary materials.

Method	Pre-train data	Input	Crops	Params	FLOPs	Top-1	Top-5
VideoMambaPro-Ti	IN-1K	32×224^2	4×3	7M	0.4T	85.8 (+7.0)	96.9 (+3.0)
VideoMambaPro-S	IN-1K	32×224^2	4×3	24M	1.5T	88.5 (+7.0)	98.1 (+2.9)
VideoMambaPro-M	IN-1K	32×224^2	4×3	69M	4.6T	90.3 (+7.9)	98.5 (+2.8)
VideoMambaPro-Ti	IN-1K+CLIP-400M	32×224^2	4×3	7M	0.4T	87.0 (+8.2)	97.3 (+3.4)
VideoMambaPro-S	IN-1K+CLIP-400M	32×224^2	4×3	24M	1.5T	90.0 (+6.9)	98.4 (+2.4)
VideoMambaPro-M	IN-1K+CLIP-400M	32×224^2	4×3	69M	4.6T	91.7 (+7.8)	98.9 (+2.7)
VideoMambaPro-Ti	IN-1K+CLIP-400M	32×384^2	4×3	7M	1.0T	87.5 (+6.4)	97.4 (+2.2)
VideoMambaPro-S	IN-1K+CLIP-400M	32×384^2	4×3	24M	3.7T	90.2 (+6.2)	98.4 (+2.2)
VideoMambaPro-M	IN-1K+CLIP-400M	32×384^2	4×3	69M	13.3T	91.9 (+7.2)	98.9 (+2.1)

Table 5: Results on K400 for various model sizes, pre-train data, and input sizes. Improvements over VideoMamba appear in parentheses in the last two columns. Best results in **bold**.

We investigate the relative performance per class when using VideoMambaPro-M with 224^2 image size pre-trained on IN-1K dataset, compared to a VideoMamba-M baseline with the same settings. We show the relative performance for all classes of Kinetics-400 in Figure 2. For over 95% of the classes, VideoMambaPro shows improvement. Although there is a lower performance for certain classes, the decrease is typically limited.

The majority of the classes sees a 6-10% improvement, which is substantial. For a small number of classes, VideoMambaPro performs >10% better than VideoMamba.

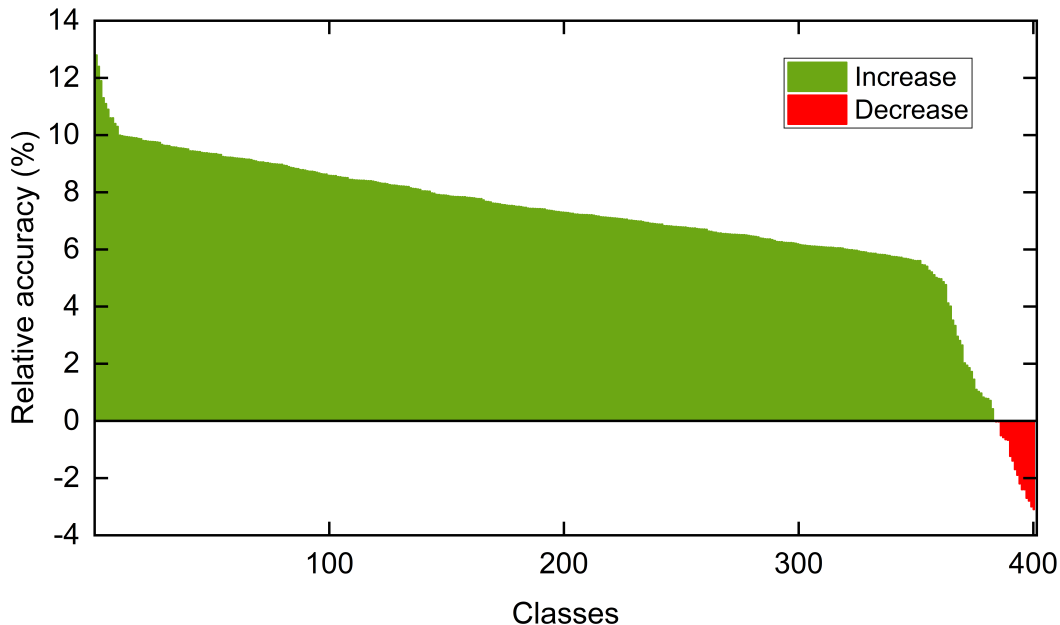


Figure 2: Relative accuracy per class on Kinetics-400 by comparing VideoMambaPro-M to a baseline VideoMamba-M. Classes sorted by relative performance.

5.4 Statistical comparison between VideoMamba and VideoMambaPro results

In order to understand whether the improvements of VideoMambaPro over VideoMamba are statistically significant, we compare the results of the respective Middle models, both pre-trained on ImageNet-1K and with a spatial input size of 224×224 . Other settings are also the same. For each test sample, we check whether it correctly classified by either model, irrespective of the class. The summary of these results appears in Table 6.

		VideoMambaPro-M		
		True	False	Total
VideoMamba-M	True	15,900	502	16,402
	False	2,075	1,429	3,504
Total		17,975	1,931	19,906

Table 6: Contingency table for test items for VideoMamba-M and VideoMambaPro-M.

Based on these results, we calculate the McNemar test, which is a non-parametric test with a single degree of freedom. Essentially, it checks whether the number of items that are incorrectly classified by VideoMambaPro-M but not VideoMamba is substantially lower than the number of items misclassified by VideoMamba but not VideoMambaPro. The McNemar test is calculated as $\chi^2 = \frac{(n_{01} - n_{10})^2}{(n_{01} + n_{10})}$ with n_{01} corresponding to the number of items that were misclassified by VideoMamba but not VideoMambaPro, and n_{10} the number of items that were correctly classified by VideoMamba but misclassified by VideoMambaPro. These numbers correspond to 2,075 and 502, respectively. Based on the Chi-square distribution, the resulting value of 12,573 corresponds to a significance level of $p < 0.001$. We can thus conclude that VideoMambaPro-M is statistically significantly better than VideoMamba.

Because we relied on the performance reported in papers for other methods, we cannot report statistical comparisons here.

5.5 Ablation: masked backward computation and residual connections

We have identified two limitations that exist in VideoMamba, historical decay and element contradiction, and have introduced masked backward computation and residual connections to address these, respectively. Here, we examine the contribution of each innovation separately and jointly. We use the same settings as in the previous section, with VideoMambaPro-M and pre-training on the IN-1K+CLIP-400M dataset. We summarize the performance of VideoMambaPro-M on Kinetic-400 in Table 7.

Both innovations result in improvements over the VideoMamba-M baseline. Using residual connections in the bi-directional Mamba block increases the top-1 accuracy by 3.3%, whereas using masked backward computation adds 4.5% top-1 accuracy. Importantly, these gains are partly independent, as witnessed from the increased when comparing these results to the full model with both innovations applied. Similar observations are made when examining the top-5 accuracy, albeit with smaller effects.

Models	Pretrain	Input	Top-1	Top-5
VideoMamba-M (baseline)	IN-1K+CLIP-400M	32×2242	83.9	96.2
VideoMambaPro-M (w/o residual connection)	IN-1K+CLIP-400M	32×2242	87.2 (+3.3)	97.8 (+1.6)
VideoMambaPro-M (w/o masked backward computation)	IN-1K+CLIP-400M	32×2242	88.4 (+4.5)	98.0 (+1.8)
VideoMambaPro-M (full model)	IN-1K+CLIP-400M	32×2242	91.7 (+7.8)	98.9 (+2.7)

Table 7: Ablation study to investigate the effect of using masked backward computation and residual connections in the bi-directional Mamba block.

5.6 Computation cost comparison

We compare the performance of our VideoMambaPro-M with and without pre-training and with two input sizes with other approaches on Kinetics-400. We visually map the top-1 accuracy against the number of parameters and FLOPs in Figures 3 and 4, respectively. VMP-A is the VideoMambaPro-M model with additional training on CLIP-400 and VMP-A+L is VideoMambaPro-M with additional training and larger input size. The details of these models appear in Table 5.

VideoMambaPro’s performance is only superseded by InternVideo and InternVideo2, but these come with a substantially larger number of parameters and FLOPs. The number of parameters for EVL-L (67M) is comparable to VideoMambaPro-M (69M) but the number of FLOPs is a factor 4 higher. Moreover, the performance of EVL-L is 4.2% lower. Overall, our VideoMambaPro achieves performance on par with the state-of-the-art at computationally very competitive performance.

6 Conclusion

From a mathematical comparison with self-attention, we have identified two limitations in how Mamba processes token sequences. We argue that these limitations constrain Mamba’s potential, especially in video understanding tasks. To this end, we have introduced VideoMambaPro (VMP), which takes VideoMamba and introduces the masked backward State Space Model (SSM), and adds residual connections in both forward and backward SSM to address the two limitations. In experiments on Kinetics-400, Something-Something V2, HMDB51, UCF-101, and AVA V2.2, VideoMambaPro consistently demonstrates state-of-the-art or competitive performance, but with significantly lower computation cost. For example, with a top-1 performance of 91.9% on Kinetics-400, we perform only 0.2% lower than the recent InternVideo-6B, but with only 1.2% of the parameters. This combination of high performance and efficiency makes VideoMambaPro a promising solution for video understanding tasks.

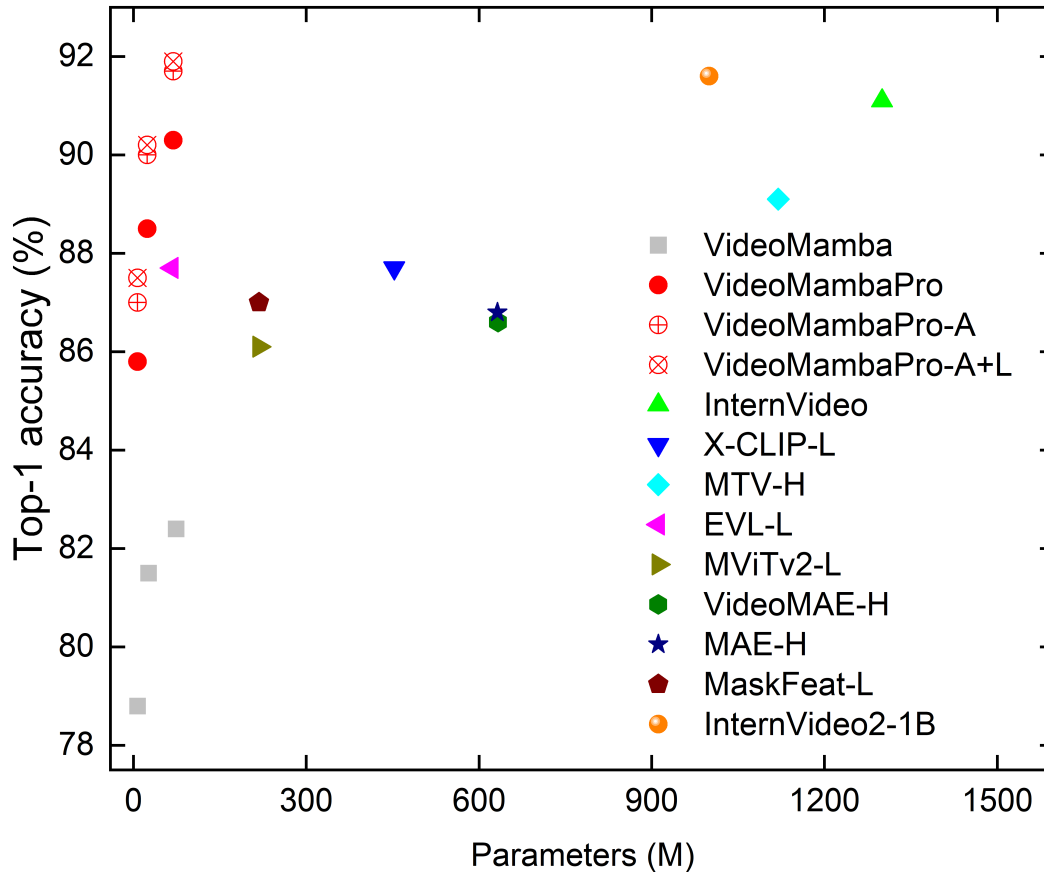


Figure 3: Top-1 accuracy versus number of parameters of VideoMambaPro and other models on Kinetics-400.

References

- [1] Alayrac, J.B., Recasens, A., Schneider, R., Arandjelović, R., Ramapuram, J., De Fauw, J., Smaira, L., Dieleman, S., Zisserman, A.: Self-supervised multimodal versatile networks. *NeurIPS* **33**, 25–37 (2020)
- [2] Alwassel, H., Mahajan, D., Korbar, B., Torresani, L., Ghanem, B., Tran, D.: Self-supervised learning by cross-modal audio-video clustering. *NeurIPS* **33**, 9758–9770 (2020)
- [3] Carreira, J., Zisserman, A.: Quo vadis, action recognition? A new model and the Kinetics dataset. In: *CVPR*. pp. 6299–6308 (2017)
- [4] Diba, A., Sharma, V., Safdari, R., Lotfi, D., Sarfraz, S., Stiefelhagen, R., Van Gool, L.: Vi2CLR: Video and image for visual contrastive learning of representation. In: *CVPR*. pp. 1502–1512 (2021)
- [5] Dosovitskiy, A., Beyer, L., Kolesnikov, A., Weissenborn, D., Zhai, X., Unterthiner, T., Dehghani, M., Minderer, M., Heigold, G., Gelly, S., Uszkoreit, J., Houlsby, N.: An image is worth 16x16 words: Transformers for image recognition at scale. In: *ICLR* (2021)
- [6] Fang, Y., Liao, B., Wang, X., Fang, J., Qi, J., Wu, R., Niu, J., Liu, W.: You only look at one sequence: Rethinking transformer in vision through object detection. *NeurIPS* **34**, 26183–26197 (2021)
- [7] Faure, G.J., Chen, M.H., Lai, S.H.: Holistic interaction transformer network for action detection. In: *WACV*. pp. 3340–3350 (2023)

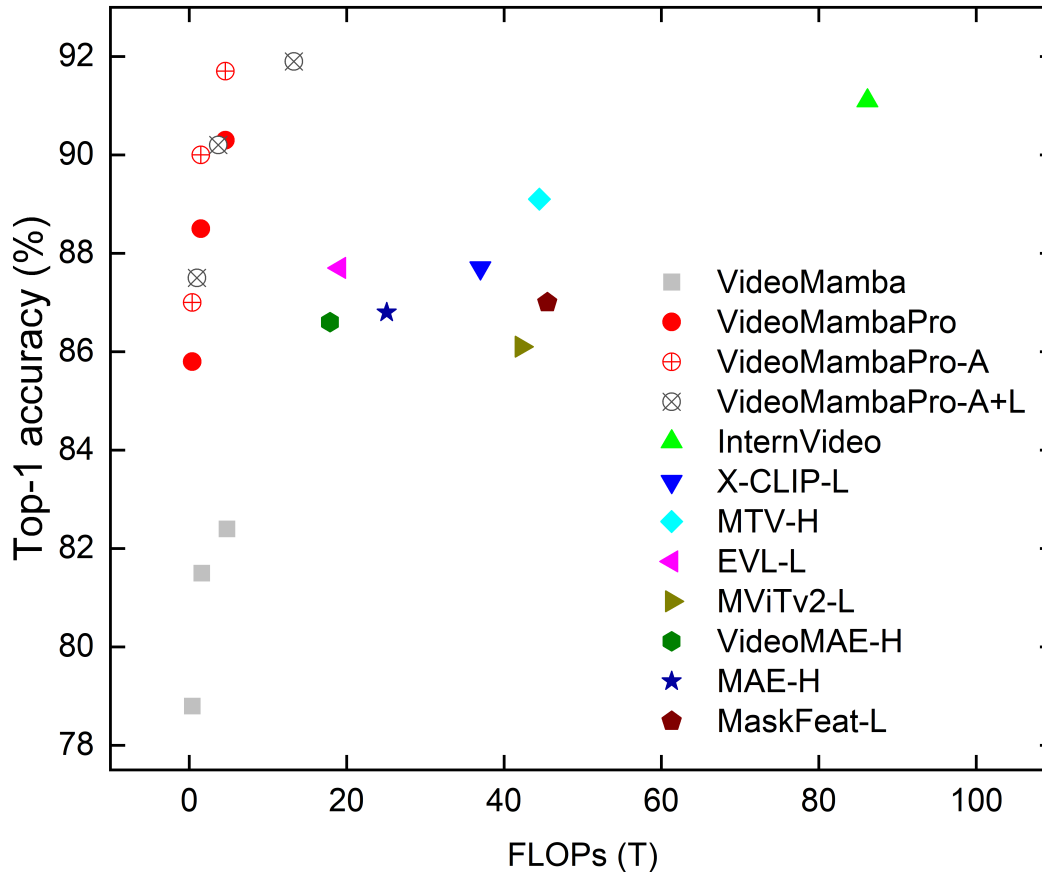


Figure 4: Top-1 accuracy versus number of FLOPs of VideoMambaPro and other models on Kinetics-400.

- [8] Feichtenhofer, C., Fan, H., Li, Y., He, K.: Masked autoencoders as spatiotemporal learners. *NeurIPS* **35**, 35946–35958 (2022)
- [9] Feichtenhofer, C., Fan, H., Malik, J., He, K.: Slowfast networks for video recognition. In: *ICCV*. pp. 6202–6211 (2019)
- [10] Goyal, R., Ebrahimi Kahou, S., Michalski, V., Materzynska, J., Westphal, S., Kim, H., Haanel, V., Freund, I., Yianilos, P., Mueller-Freitag, M., et al.: The "Something Something" video database for learning and evaluating visual common sense. In: *ICCV*. pp. 5842–5850 (2017)
- [11] Gu, A., Dao, T.: Mamba: Linear-time sequence modeling with selective state spaces. *arXiv preprint arXiv:2312.00752* (2023)
- [12] Gu, A., Dao, T., Ermon, S., Rudra, A., Ré, C.: Hippo: Recurrent memory with optimal polynomial projections. *NeurIPS* **33**, 1474–1487 (2020)
- [13] Gu, A., Goel, K., Ré, C.: Efficiently modeling long sequences with structured state spaces. *arXiv preprint arXiv:2111.00396* (2021)
- [14] Gu, C., Sun, C., Ross, D.A., Vondrick, C., Pantofaru, C., Li, Y., Vijayanarasimhan, S., Toderici, G., Ricco, S., Sukthankar, R., et al.: AVA: A video dataset of spatio-temporally localized atomic visual actions. In: *CVPR*. pp. 6047–6056 (2018)
- [15] Han, T., Xie, W., Zisserman, A.: Memory-augmented dense predictive coding for video representation learning. In: *ECCV*. pp. 312–329 (2020)
- [16] Hu, K., Shao, J., Liu, Y., Raj, B., Savvides, M., Shen, Z.: Contrast and order representations for video self-supervised learning. In: *ICCV*. pp. 7939–7949 (2021)

- [17] Keles, F.D., Wijewardena, P.M., Hegde, C.: On the computational complexity of self-attention. In: International Conference on Algorithmic Learning Theory. pp. 597–619. PMLR (2023)
- [18] Kuehne, H., Jhuang, H., Garrote, E., Poggio, T., Serre, T.: HMDB: a large video database for human motion recognition. In: ICCV. pp. 2556–2563 (2011)
- [19] Li, K., Li, X., Wang, Y., He, Y., Wang, Y., Wang, L., Qiao, Y.: VideoMamba: State space model for efficient video understanding. arXiv preprint arXiv:2403.06977 (2024)
- [20] Li, K., Wang, Y., He, Y., Li, Y., Wang, Y., Wang, L., Qiao, Y.: UniformerV2: Spatiotemporal learning by arming image vits with video uniformer. arXiv preprint arXiv:2211.09552 (2022)
- [21] Li, K., Wang, Y., Li, Y., Wang, Y., He, Y., Wang, L., Qiao, Y.: Unmasked teacher: Towards training-efficient video foundation models. In: ICCV. pp. 19948–19960 (2023)
- [22] Li, K., Wang, Y., Peng, G., Song, G., Liu, Y., Li, H., Qiao, Y.: Uniformer: Unified transformer for efficient spatial-temporal representation learning. In: ICLR (2022)
- [23] Li, W., Hong, X., Fan, X.: Spikemba: Multi-modal spiking saliency mamba for temporal video grounding. arXiv preprint arXiv:2404.01174 (2024)
- [24] Li, Y., Wu, C.Y., Fan, H., Mangalam, K., Xiong, B., Malik, J., Feichtenhofer, C.: MViTv2: Improved multiscale vision transformers for classification and detection. In: CVPR. pp. 4804–4814 (2022)
- [25] Lin, Z., Geng, S., Zhang, R., Gao, P., de Melo, G., Wang, X., Dai, J., Qiao, Y., Li, H.: Frozen clip models are efficient video learners. In: ECCV. pp. 388–404 (2022)
- [26] Liu, Q., Xu, Z., Bertasius, G., Niethammer, M.: SimpleClick: Interactive image segmentation with simple vision transformers. In: ICCV. pp. 22290–22300 (2023)
- [27] Liu, Y., Tian, Y., Zhao, Y., Yu, H., Xie, L., Wang, Y., Ye, Q., Liu, Y.: VMamba: Visual state space model. arXiv preprint arXiv:2401.10166 (2024)
- [28] Loshchilov, I., Hutter, F.: Decoupled weight decay regularization. arXiv preprint arXiv:1711.05101 (2017)
- [29] Lu, H., Jian, H., Poppe, R., Salah, A.A.: Enhancing video transformers for action understanding with vlm-aided training. arXiv preprint arXiv:2403.16128 (2024)
- [30] Lu, J., Yao, J., Zhang, J., Zhu, X., Xu, H., Gao, W., Xu, C., Xiang, T., Zhang, L.: Soft: Softmax-free transformer with linear complexity. NeurIPS **34**, 21297–21309 (2021)
- [31] Mehta, H., Gupta, A., Cutkosky, A., Neyshabur, B.: Long range language modeling via gated state spaces. arXiv preprint arXiv:2206.13947 (2022)
- [32] Ni, B., Peng, H., Chen, M., Zhang, S., Meng, G., Fu, J., Xiang, S., Ling, H.: Expanding language-image pretrained models for general video recognition. In: ECCV. pp. 1–18 (2022)
- [33] Pan, T., Song, Y., Yang, T., Jiang, W., Liu, W.: VideoMoCo: Contrastive video representation learning with temporally adversarial examples. In: CVPR. pp. 11205–11214 (2021)
- [34] Patrick, M., Asano, Y.M., Fong, R., Henriques, J.F., Zweig, G., Vedaldi, A.: Multi-modal self-supervision from generalized data transformations. arXiv preprint arXiv:2003.04298 (2020)
- [35] Patro, B.N., Agneeswaran, V.S.: Mamba-360: Survey of state space models as transformer alternative for long sequence modelling: Methods, applications, and challenges. arXiv preprint arXiv:2404.16112 (2024)
- [36] Peng, B., Alcaide, E., Anthony, Q., Albalak, A., Arcadinho, S., Cao, H., Cheng, X., Chung, M., Grella, M., GV, K.K., et al.: RWKV: Reinventing RNNs for the transformer era. arXiv preprint arXiv:2305.13048 (2023)
- [37] Piergiovanni, A., Kuo, W., Angelova, A.: Rethinking video ViTs: Sparse video tubes for joint image and video learning. In: CVPR. pp. 2214–2224 (2023)

- [38] Qian, R., Meng, T., Gong, B., Yang, M.H., Wang, H., Belongie, S., Cui, Y.: Spatiotemporal contrastive video representation learning. In: CVPR. pp. 6964–6974 (2021)
- [39] Rajasegaran, J., Pavlakos, G., Kanazawa, A., Feichtenhofer, C., Malik, J.: On the benefits of 3D pose and tracking for human action recognition. In: CVPR. pp. 640–649 (2023)
- [40] Ren, H., Dai, H., Dai, Z., Yang, M., Leskovec, J., Schuurmans, D., Dai, B.: Combiner: Full attention transformer with sparse computation cost. *NeurIPS* **34**, 22470–22482 (2021)
- [41] Ryali, C., Hu, Y.T., Bolya, D., Wei, C., Fan, H., Huang, P.Y., Aggarwal, V., Chowdhury, A., Poursaeed, O., Hoffman, J., et al.: Hiera: A hierarchical vision transformer without the bells-and-whistles. *arXiv preprint arXiv:2306.00989* (2023)
- [42] Shen, Y., Lai, E.M.K., Mohaghegh, M.: Effects of similarity score functions in attention mechanisms on the performance of neural question answering systems. *Neural Processing Letters* **54**(3), 2283–2302 (2022)
- [43] Soomro, K., Zamir, A.R., Shah, M.: UCF101: A dataset of 101 human actions classes from videos in the wild. *arXiv preprint arXiv:1212.0402* (2012)
- [44] Strudel, R., Garcia, R., Laptev, I., Schmid, C.: Segmenter: Transformer for semantic segmentation. In: ICCV. pp. 7262–7272 (2021)
- [45] Sun, Y., Dong, L., Huang, S., Ma, S., Xia, Y., Xue, J., Wang, J., Wei, F.: Retentive network: A successor to transformer for large language models. *arXiv preprint arXiv:2307.08621* (2023)
- [46] Tan, H., Lei, J., Wolf, T., Bansal, M.: Vimpac: Video pre-training via masked token prediction and contrastive learning. *arXiv preprint arXiv:2106.11250* (2021)
- [47] Tong, Z., Song, Y., Wang, J., Wang, L.: VideoMAE: Masked autoencoders are data-efficient learners for self-supervised video pre-training. *NeurIPS* **35**, 10078–10093 (2022)
- [48] Touvron, H., Cord, M., Douze, M., Massa, F., Sablayrolles, A., Jégou, H.: Training data-efficient image transformers & distillation through attention. In: ICML. pp. 10347–10357. PMLR (2021)
- [49] Vaswani, A., Shazeer, N., Parmar, N., Uszkoreit, J., Jones, L., Gomez, A.N., Kaiser, Ł., Polosukhin, I.: Attention is all you need. *NeurIPS* **30** (2017)
- [50] Wang, L., Huang, B., Zhao, Z., Tong, Z., He, Y., Wang, Y., Wang, Y., Qiao, Y.: VideoMAE V2: Scaling video masked autoencoders with dual masking. In: CVPR. pp. 14549–14560 (2023)
- [51] Wang, R., Chen, D., Wu, Z., Chen, Y., Dai, X., Liu, M., Jiang, Y.G., Zhou, L., Yuan, L.: BEVT: Bert pretraining of video transformers. In: CVPR. pp. 14733–14743 (2022)
- [52] Wang, R., Chen, D., Wu, Z., Chen, Y., Dai, X., Liu, M., Yuan, L., Jiang, Y.G.: Masked video distillation: Rethinking masked feature modeling for self-supervised video representation learning. In: CVPR. pp. 6312–6322 (2023)
- [53] Wang, Y., Li, K., Li, X., Yu, J., He, Y., Chen, G., Pei, B., Zheng, R., Xu, J., Wang, Z., et al.: InternVideo2: Scaling video foundation models for multimodal video understanding. *arXiv preprint arXiv:2403.15377* (2024)
- [54] Wang, Y., Li, K., Li, Y., He, Y., Huang, B., Zhao, Z., Zhang, H., Xu, J., Liu, Y., Wang, Z., et al.: InternVideo: General video foundation models via generative and discriminative learning. *arXiv preprint arXiv:2212.03191* (2022)
- [55] Wei, C., Fan, H., Xie, S., Wu, C.Y., Yuille, A., Feichtenhofer, C.: Masked feature prediction for self-supervised visual pre-training. In: CVPR. pp. 14668–14678 (2022)
- [56] Yan, S., Xiong, X., Arnab, A., Lu, Z., Zhang, M., Sun, C., Schmid, C.: Multiview transformers for video recognition. In: CVPR. pp. 3333–3343 (2022)
- [57] Zhang, H., Zhu, Y., Wang, D., Zhang, L., Chen, T., Ye, Z.: A survey on Visual Mamba. *arXiv preprint arXiv:2404.15956* (2024)

- [58] Zhang, Z., Chong, K.T.: Comparison between first-order hold with zero-order hold in discretization of input-delay nonlinear systems. In: 2007 International Conference on Control, Automation and Systems. pp. 2892–2896 (2007)
- [59] Zhang, Z., Lu, X., Cao, G., Yang, Y., Jiao, L., Liu, F.: ViT-YOLO: Transformer-based YOLO for object detection. In: ICCV. pp. 2799–2808 (2021)
- [60] Zhu, C., Ping, W., Xiao, C., Shoeybi, M., Goldstein, T., Anandkumar, A., Catanzaro, B.: Long-short transformer: Efficient transformers for language and vision. *NeurIPS* **34**, 17723–17736 (2021)
- [61] Zhu, L., Wang, X., Ke, Z., Zhang, W., Lau, R.W.: BiFormer: Vision transformer with bi-level routing attention. In: CVPR. pp. 10323–10333 (2023)
- [62] Zhu, L., Liao, B., Zhang, Q., Wang, X., Liu, W., Wang, X.: Vision Mamba: Efficient visual representation learning with bidirectional state space model. arXiv preprint arXiv:2401.09417 (2024)

A Appendix

We provide the detailed architecture for the three VideoMambaPro models in Section A.1. A comparison between the architectures of VideoMamba and VideoMambaPro appears in Section A.2. The implementation details are shown in Section A.3.

A.1 VideoMambaPro architectures

We present the architecture details of VideoMambaPro-Tiny, -Small, and -Middle in Tables 8–10, respectively. The difference are in the embedding dimension (192, 384, 576) and the number of SSM blocks (24, 24, 32).

Stage	Tiny
Patch Embedding	nn.Conv3d (kernel size = $16 \times 16 \times 1$, embedding dimension = 192)
SSM	$\begin{bmatrix} \text{MLP}(768) \\ \text{MLP}(3072) \\ \text{MHA} (\text{head} = 12) \end{bmatrix} \times 24$
Projection	Layer Normalization Dropout (ratio) Linear layer (1000) Softmax

Table 8: Architecture details of VideoMambaPro-Ti.

Stage	Small
Patch Embedding	nn.Conv3d (kernel size = $16 \times 16 \times 1$, embedding dimension = 384)
SSM	$\begin{bmatrix} \text{MLP}(768) \\ \text{MLP}(3072) \\ \text{MHA} (\text{head} = 12) \end{bmatrix} \times 24$
Projection	Layer Normalization Dropout (ratio) Linear layer (1000) Softmax

Table 9: Architecture details of VideoMambaPro-S.

Stage	Middle
Patch Embedding	nn.Conv3d (kernel size = $16 \times 16 \times 1$, embedding dimension = 576)
SSM	$\begin{bmatrix} \text{MLP}(768) \\ \text{MLP}(3072) \\ \text{MHA} (\text{head} = 12) \end{bmatrix} \times 32$
Projection	Layer Normalization Dropout (ratio) Linear layer (1000) Softmax

Table 10: Architecture details of VideoMambaPro-M.

A.2 Architecture comparison with VideoMamba

We compare the architectures of VideoMambaPro and VideoMamba in Figure 5. Compared to VideoMamba, VideoMambaPro does not have the linear layer to generate parameters z . Additionally, our residual SSM and mask scheme do not introduce additional parameters or computational overhead, so our method has slightly fewer parameters and FLOPs.

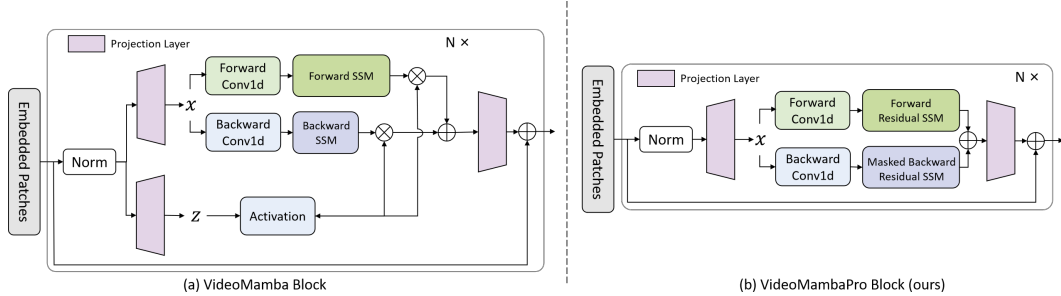


Figure 5: Comparison between the bi-directional VideoMamba (left) and VideoMambaPro (right) blocks.

A.3 Implementation details

We conduct the experiments with 16 NVIDIA A100-80G GPUs for both pre-training on ImageNet-1K and fine-tuning on the Something-Something V2 and Kinetics-400 datasets. The experiments on the smaller UCF101 and HMDB51 datasets are trained with 8 A100-80G GPUs. The experiments on the AVA dataset are conducted with 32 A100-80G GPUs. The values of the hyperparameters is largely similar to those used in VideoMamba. We linearly scale the base learning rate with respect to the overall batch size, $lr = lr_{base} \times batchsize/256$. The pre-training details are shown in Table 11, and the fine-tuning details on Kinetics-400, SSv2, UCF101, HMDB51, and AVA V2.2 are listed in Tables 12–15.

config	image size: 224×224
optimizer	AdamW
base learning rate	$1.5e-4$
weight decay	0.1 (Tiny), 0.05 (Small, Middle)
minimal learning rate	$1.0e-6$
optimizer momentum	$\beta_1, \beta_2 = 0.9, 0.95$
batch size	512
learning rate schedule	cosine decay
warmup epochs	5 (Tiny), 10 (Small), 40 (Middle)
dropout ratio	0 (Tiny), 0.15 (Small), 0.5 (Middle)
augmentation	MultiScaleCrop
label smoothing	0.1

Table 11: Pre-training setting on ImageNet-1K

config	image size: 224×224
optimizer	AdamW
base learning rate	$1.5e-4$
weight decay	0.1 (Tiny), 0.05 (Small, Middle)
minimal learning rate	$1.0e-6$
optimizer momentum	$\beta_1, \beta_2 = 0.9, 0.99$
batch size	256
learning rate schedule	cosine decay
warmup epochs	5 (Tiny), 5 (Small) 10 (Middle)
dropout ratio	0.1 (Tiny), 0.35 (Small), 0.6 (Middle)
augmentation	RandAug (7, 0.25) (Tiny), RandAug (9, 0.5) (Small, Middle)
label smoothing	0.1
flip augmentation	yes

Table 12: Fine-tuning setting for Kinetics-400

config	image size: 224 × 224
optimizer	AdamW
base learning rate	4e-4
weight decay	0.1 (Tiny), 0.05 (Small, Middle)
minimal learning rate	1.0e-6
optimizer momentum	$\beta_1, \beta_2 = 0.9, 0.999$
batch size	256
learning rate schedule	cosine decay
warmup epochs	5 (Tiny), 5 (Small) 10 (Middle)
dropout ratio	0.1 (Tiny), 0.35 (Small), 0.6 (Middle)
augmentation	RandAug (7, 0.25) (Tiny), RandAug (9, 0.5) (Small, Middle)
label smoothing	0.1
flip augmentation	no

Table 13: Fine-tuning setting for SSv2

config	image size: 224 × 224
optimizer	AdamW
base learning rate	4e-4
weight decay	0.1 (Tiny), 0.05 (Small, Middle)
minimal learning rate	1.0e-6
optimizer momentum	$\beta_1, \beta_2 = 0.9, 0.99$
batch size	128
learning rate schedule	cosine decay
warmup epochs	5 (Tiny), 5 (Small) 10 (Middle)
dropout ratio	0.1 (Tiny), 0.35 (Small), 0.6 (Middle)
augmentation	RandAug (7, 0.25) (Tiny), RandAug (9, 0.5) (Small, Middle)
label smoothing	0.1
flip augmentation	yes

Table 14: Fine-tuning setting for UCF101/HMDB51

config	image size: 224 × 224
optimizer	AdamW
base learning rate	1.5e-3 (Tiny), 2.5e-4 (Small, Middle)
weight decay	0.051 (Tiny, Small, Middle)
minimal learning rate	1.0e-6
optimizer momentum	$\beta_1, \beta_2 = 0.9, 0.999$
batch size	128
learning rate schedule	cosine decay
warmup epochs	5 (Tiny), 5 (Small) 10 (Middle)
dropout ratio	0.1 (Tiny), 0.35 (Small) 0.6 (Middle)
augmentation	RandAug (7, 0.25) (Tiny), RandAug (9, 0.5) (Small, Middle)
label smoothing	0.1
flip augmentation	yes

Table 15: Fine-tuning setting for AVA 2.2